Phys. Status Solidi A **209,** No. 8, 1583–1587 (2012) / **DOI** 10.1002/pssa.201127741

physica status solidi a
www.pss-a.com
applications and materials science

Improved efficiency of hybrid solar cell based on thiols-passivated CdS quantum dots and poly(3-hexythiophene)

Xinmei Liu[1,2], Yang Jiang*[,1], Xinzheng Lan[1], Yugang Zhang[1], Chao Liu[1], Junwei Li[1], Binbin Wang[1], Yongqiang Yu[1], and Wenjun Wang[1]

[1] School of Materials Science and Engineering, Hefei University of Technology, Hefei, Anhui 230009, P. R. China
[2] Department of Biological and Chemical Engineering, Guangxi University of Technology, Liuzhou, Guangxi 545006, P. R. China

Received 16 December 2011, revised 16 April 2012, accepted 19 April 2012
Published online 18 May 2012

Keywords cadmium sulphide, colloidal processing, hybrid solar cells, polymers, quantum dots

* Corresponding author: e-mail apjiang@hfut.edu.cn, Phone: +86 551 2904358, Fax: +86 551 2904358

A bulk-heterojunction hybrid solar cell based on CdS quantum dots (QDs) as electron acceptor and P3HT as donor was fabricated for the first time. The CdS QDs synthesized by a one-pot method had good crystallinity and stability. The hybrid thin film of CdS-QDs and conjugated polymer was made by simple spin-coating deposition of CdS-QDs/P3HT composite solution on ITO substrates and then treated by bidentate ligand ethanedithiol. Under AM1.5G illumination, the power-conversion efficiency (PCE) of the thiol-treated monolayer film was more than three times higher than that of the untreated device. The hybrid solar cell based on the assembled trilayer blend film with ethanedithiol by a layer-by-layer approach exhibited a further improved PCE of 0.86%, which was sixfold higher than that of the thiol-treated monolayer device. The results can be explained via ethanedithiol effectively displacing the existing stearate ligands on the surface of QDs in situ and connecting nanoparticles by its end function group, shortening the interdot space and thus improving electron transport between the QDs. The morphology of the thiol-treated blend film was briefly investigated.

1 Introduction Solar cells based on conjugated polymers offer great potential in solar energy conversion in view of their compatibility with solution processing, enabling rapid, large-area, low-cost fabrication [1, 2]. The state-of-the art power-conversion efficiency (PCE) of solar cells based on conjugated polymers has already been reported to reach 6.5% [3]. A hybrid polymer–inorganic solar cell, in which inorganic semiconductor nanocrystals were used as electron acceptors in conjugated-based solar cells, is believed to exhibit greater potentialities in further improving the device performance due to combining the advantages of both types of materials: the solution processing of the polymer semiconductor and the high charge-carrier mobility of inorganic semiconductor [4, 5]. In addition, the semiconductor nanocrystal quantum confinement effect allows one to tune the visible response and vary the band offsets to modulate the vectorial charge transfer across different sized particles [6, 7].

However, despite the advantage with respect to light absorption and electron transports, the maximum PCE for cells containing inorganic nanocrystals–polymer photoactive layers is much lower than that for all-organic solar cell so far. The main factor responsible for the relatively poor PCE of such hybrid solar cells may be due to the greater tendency of the inorganic nanoparticles to aggregate during the solvent evaporation compared to C60-derivates resulting in an insufficient control over the morphology of the photoactive layer [8]. In most cases, the inert stabilizers containing long alkyl chains used for preventing aggregation of the quantum dots (QDs) forbid the formation of an efficient interface between nanoparticles and a hole-transporting polymer. Poor interfacial contact between nanoparticle/polymer will enhance recombination and decrease charge-separation efficiency, causing a decrease of PCE.

In the bulk-heterojunction (BHJ) cells, the nanocrystals should be ligand-free within the photoactive layer. In order to improve the charge transfer between QDs and polymer, as well as electron transport between NCs, removal of the stabilizing agents is needed through ligand exchange. For example, pyridine treatment of the QDs is the most

commonly used and effective procedure for improving device efficiency [9]. Repeated pyridine treatment enabled more efficient charge transfer. However, a study suggests that the repeated pyridine treatment up to three times not only cannot completely remove the alkyl chains, instead of decreasing the PCE of the solar cells due to the increase of aggregation influencing the morphology of the blends, and a larger amount of surface defects existing in particles when they were stabilized by the weak pyridine ligand shell [10].

The use of thiol-terminated ligands to passivate the nanocrystals surface has recently been reported to dramatically enhance the PCE of the Pb*E* (*E* = S,Se)-based Schottky solar cells. The beneficial effects of short-chain thiol treatment on PV device performance have been substantially attributed to a shortening of interdot distance, improved crosslinking of dots, and an improvement in carrier collection [11, 12].

In this study, we fabricated a hybrid solar cell device based on CdS QDs and P3HT blends, on which very few reports are available. The CdS QDs synthesized by one-pot method had good optical properties, crystallinity, and storage stability. The hybrid solar cell was fabricated by a simple spin-coating deposition method. Bidentate ligands ethanedithiol was used to treat and assemble in situ the photoactive layer consisting of CdS QDs and P3HT blends. A significantly improved PCE was obtained. Additionally, the morphology of blend film was roughly studied through atomic force microscopy (AFM), field-emission scanning electron microcopy (FESEM), and electron energy loss spectroscopy (EELS).

2 Experimental section

2.1 Materials Pyridine, chlorobenzene (CBZ), ethanedithiol, and acetonitrile were purchased from Sinopharm Chemical Reagents Co. Ltd. P3HT (Mn = 45,000–65,000, 99.995%) was purchased from Sigma-Aldrich. The CdS QDs were prepared by a one-pot method described in literature [13]. The purified CdS QDs samples used for fabrication of hybrid solar cells were refluxed for 24 h in pyridine twice and centrifuged out with hexane to replace the long alkyl chain ligands, as reported previously [10]. The QDs after ligand exchange were dissolved in CBZ and mixed with P3HT CBZ solution for the fabrication of blend film.

2.2 Device preparation Devices were fabricated on indium tin oxide (ITO, 15 Ω/square) coated glass substrates. To avoid local short circuits, half of the ITO coating was etched away with HCl and zinc powder. Subsequently, the substrates were cleaned with detergent, deionized water, acetone, and isopropanol in turn in an ultrasonic bath and then dried under a stream of Ar. A 30-nm thick layer of PEDOT:PSS (poly(3,4-ethylene-dioxythiophene)-poly-(styrenesulfonate), Baytron P 4083) was first spin coated onto the cleaned ITO substrates and was dried at 120 °C for 30 min in a vacuum oven. On top of the PEDOT:PSS film, the active layer was deposited by spin coating the mixed solution of CdS-QDs/P3HT under an inert atmosphere. If the ethanedithiol treatment was applied, 200 μL of an ethanedithiol/acetonitrile solution (0.01%, volume ratio) was pipetted onto the surface of the as-spun films, making sure to cover the entire film [11]. After 30 s, the treatment solution was casted off and the sample dried under Ar stream. The blend film was assembled by a layer-by-layer (LBL) approach with ethanedithiol by repeating the deposition of CdS-QDs/P3HT blend film and then thiol treatment. The resulting films were annealed at 150 °C for 30 min. The selected weight ratio of P3HT to CdS QDs in the spinning solution was 1:6. Finally, shadow-mask patterned 100-nm-thick aluminum stripes were deposited on top of the blend film by electron beam evaporation. The area of the devices was 0.09 cm^2.

2.3 Characterization methods Absorption spectra were collected with a Shimadzu UV-2550 ultraviolet–visible (UV–Vis) spectrophotometer. Photoemission experiments were performed on a Hitachi F-4500 fluorescence spectrophotometer. The high-resolution transmission electron microscopy (HRTEM) images were obtained on a JEM-2100F field emission source transmission electron microscope operating at 200 kV. The current–voltage (*I–V*) curves were recorded using a Keithley 2636 sourcemeter illuminated with a solar simulator (AM1.5G, the intensity was 100 mW/cm^2). The surface morphologies were studied by AFM (CSPM4000, Being Nan. Instruments Ltd.) and FESEM (SIRION, 200, FEI). EELS data were acquired with a Gatan Tridiem imaging filter attached to the FESEM.

3 Results and discussion

3.1 Optical and structure properties of CdS QDs Figure 1 showed the UV–Vis absorption and photoluminescence (PL) spectra of the freshly prepared CdS QDs with a diameter of around 4.3 nm (calculated by Peng's empirical equation [14]) from a facile one-pot method

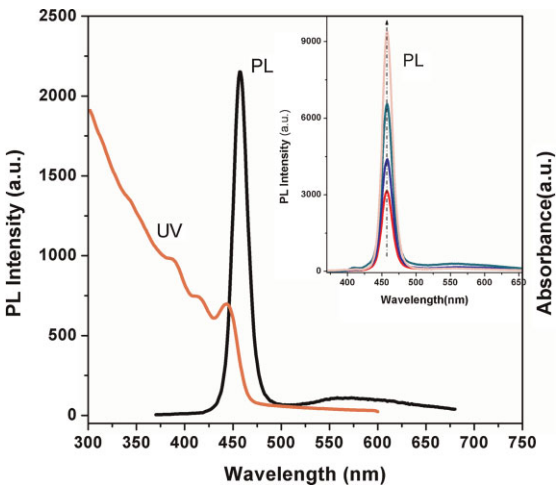

Figure 1 (online colour at: www.pss-a.com) The UV–Vis absorption and PL spectra of the freshly prepared CdS QDs sample. Inset: PL spectra of the aged CdS QDs stored in air and daylight for different time. From bottom to top, the stored time was 7, 15, 30, and 60 days, respectively. The excitation wavelength was 350 nm.

(Ref. [13]). The CdS QDs exhibited at least four absorption features and a narrow PL spectra bandwidth (the full width at half maximum (fwhm) = 18 nm), indicating the high-quality CdS QDs obtained.

The stability of the CdS QDs solution stored in air and daylight was also investigated. The inset of Fig. 1 records the change of PL intensity of the CdS QDs sample during 60-day storage periods. A significant enhancement of PL intensity was seen, not accompanied by the change of PL peak position and fwhm value. Accordingly, the quantum yield of CdS QDs was increased from 17.6 to 45.3% against Rhodamine 6G in ethanol. Further investigation suggested that the increasing PL improvement was attributed to a slow surface reconstruction of CdS QDs [13]. The UV–Vis absorption spectra of CdS QDs with different aged time are not shown due to the same peak positions, shapes, intensities, and even fine substructures as the fresh sample, which suggested that the as-prepared CdS QDs exhibited temporal stability of absorption properties. The increasing PL improvement and the invariant absorption properties make the as-prepared CdS QDs be attractive for the application of semiconductor nanocrystals in optoelectronic devices.

The typical TEM and HRTEM images (Fig. 2) showed that the as-prepared CdS QDs had good monodispersity, a quasispherical shape, and good crystallinity. The average diameter was 4.2 ± 0.3 nm. It is well known that in the QDs/polymer hybrid solar cell, the defects of the QDs will trap electrons, enhance recombination, and cause a lower PCE. The good crystallinity of semiconductor nanocrystals is believed to be of benefit for improving the electron-transport properties in the hybrid solar cell and enhancing the energy-conversion efficiency [4].

3.2 Quenching experiments Figure 3a shows the absorption spectra of CdS QDs, P3HT, and the composite solution of the CdS QDs and P3HT in CBZ, respectively. The pure CdS QDs exhibited an absorption maximum at 438 nm and the pure P3HT at 452 nm. In the spectrum of the blend, one could obviously see the contribution of both CdS QDs and P3HT to absorption.

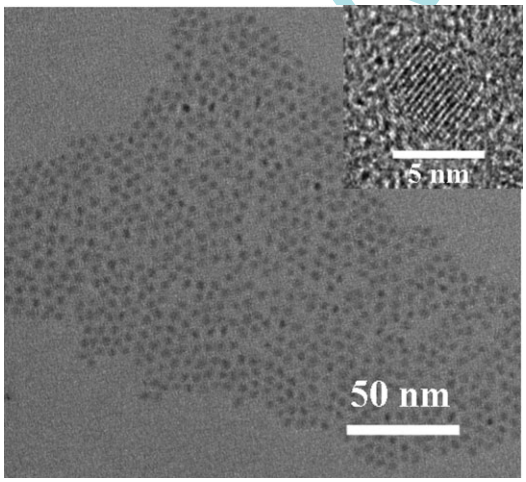

Figure 2 Typical TEM image of CdS QDs. Inset: HRTEM image of individual QDs.

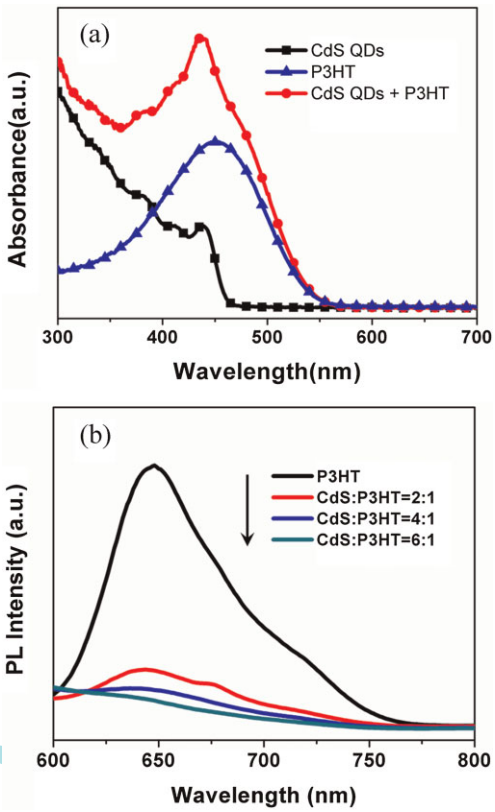

Figure 3 (online colour at: www.pss-a.com) (a) The UV–Vis absorption spectra of CdS QDs, P3HT, and CdS-QDs/P3HT composite solution in CBZ. (b) The PL spectra of CdS-QDs/P3HT blend thin film with different weight ratios of CdS-QDs to P3HT ($\lambda_{ex} = 450$ nm).

Ideal donor/acceptor interfaces are thought of as an interpenetrating nanoparticle network in three dimensions whose connected nanoparticle segments are separated by a curved polymer phase, in which a much greater area of the acceptor/donor interface is provided and the light-induced electron–hole (e–h) pairs are allowed to dissociate effectively into different phases prior to recombination. In order to estimate the charge-transfer efficiency in the CdS-QDs/P3HT composite thin films, we compared the photoluminescence yield of neat P3HT film to that of CdS-QDs/P3HT composite thin film with different amounts of CdS QDs. Figure 3b shows the PL spectra of CdS-QDs/P3HT blend film with different P3HT/CdS-QDs weight ratios of 1, 1:2, 1:4, and 1:6. For each sample, a similar spin-coating technology for the preparation of film was used to avoid thickness and geometry effects. The PL of P3HT was increasingly quenched with the increasing weight concentrations of CdS QDs, which indicated the formation of an efficient percolation network in the photoactive film and showed that Förster energy resonance transfer did not occur in the CdS/P3HT system. Then, the photoinduced e–h pairs were allowed to dissociate effectively into different phases,

electrons into CdS QDs and holes into P3HT phase. This also implied that CdS QDs were good electron acceptors in the hybrid solar cell.

3.3 Device performance The photovoltaic properties of devices made from CdS-QDs/P3HT blends were characterized by measuring *I–V* curves in the dark and under AM 1.5G simulated sunlight with an intensity of 100 mW/cm^2. Figure 4 shows the *I–V* curves of the CdS-QDs/P3HT hybrid solar cell with monolayer blend film or LBL-assembled trilayer blend films passivated by 0.01% ethanedithiol/acetonitrile solution (volume ratio).

As shown in the insets of Fig. 4a and b, the measurements carried out in the dark revealed excellent diode behavior of both devices. For comparison, the photovoltaic properties of the solar cells based on an untreated monolayer blend thin film by ethanedithiol were investigated as well. It gave a short-circuit current density (I_{SC}) of 0.65 mA/cm^2, an open-circuit voltage (V_{OC}) of 0.58 V, and a fill factor (FF) of 0.11, yielding a PCE of 0.042%. The *I–V* curve was not provided owing to the bad performance. When ethanedithiol was used to passivate the composite film, the corresponding values were $I_{SC} = 1.4$ mA/cm^2, $V_{OC} = 0.40$ V, FF = 0.26, and yielding a PCE of 0.14%. Comparing the PV performances of the two cells, it was clear that, while the V_{OC} decreased, there was a significant improvement in both I_{SC} and FF for the cell based on the treated composite film, leading to greater than threefold increase in PCE. The origin of the little photovoltaic activity and lower I_{SC} in the untreated system could be attributed to limited electron transport. Due to the absence of efficient connection, the photoinduced electron might have hopped through the CdS QDs to reach the Al electrode upon photoillumination and thus increased recombination losses. At the same time, the aggregation of CdS QDs during solvent evaporation will produce a poor morphology of the active layer, which was also related to the lower FF. It was known that the bidentate ligand ethanedithiol had a strong affinity for Cd atoms and could effectively displace the existing stearate ligands and pyridine on the surface of QDs and then connect nanoparticles through the end function group. In addition, ethanedithiol was short enough not to impede charge transport between QDs [11]. Shortening the space between the QDs improved electron transport, reduced recombination losses, and resulted in an increased PCE for the treated cell. Analogous to branched nanocrystals, QDs connected by ethanedithiol provided more extended and directed electron transmission pathways and made electron hopping more efficient between particles before the separated electrons achieved the electrode.

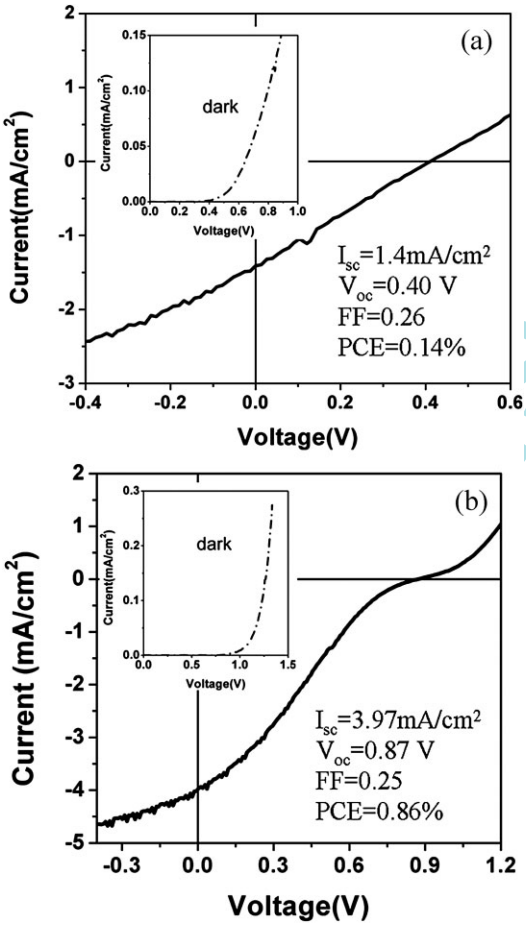

Figure 4 *I–V* curves of the CdS-QDs/P3HT hybrid solar cell with (a) monolayer blend film and (b) LBL assembled trilayer blend film passivated by 0.01% ethanedithiol/acetonitrile solution (volume ratio) under simulated AM1.5 (100 mW/cm^2) illumination. Inset: corresponding results in the dark. The weight ratio of CdS-QDs to P3HT in the two cases is 6:1.

When the sample was assembled by the LBL approach with ethanedithiol, a further increasing of PV performance was observed. The solar cells exhibited $I_{SC} = 3.97$ mA/cm^2, $V_{OC} = 0.87$ V, FF = 0.25, and PCE = 0.86%. Obviously, a thicker active layer could be obtained by the LBL-assembled approach. The film thickness measurement showed three layers of repeated LBL deposition produced about 80 nm thick films. The thicker films increased the absorption of incident light, then the photocarriers and photocurrent increased with it. This was related with the distinct improvement in both V_{OC} and I_{SC}, which led to about a sixfold increase in the PCE compared with the solar cell with monolayer film. It is a pity that the thiol could not bridge the conjugated polymer and semiconductor nanocrystals like the LBL approach driven by covalent coupling reactions, in which a functional group was used to crosslink polymers and semiconductor nanocrystals, and the bridged acceptor and donor is favorable for electron and hole transport [15, 16]. It was worth noting that the FF was relatively low, 25%. Generally, low FF can be induced by high series resistances and/or by small shunt resistances. Obviously, the high series resistance was shown with the slope at $I = 0$ mA/cm^2 point and the low parallel shunt resistances with the slope at 0 V point in *I–V* curves of Fig. 4. The former was possibly related with inferior interfacial contacts between the photoactive layers and the electrodes.

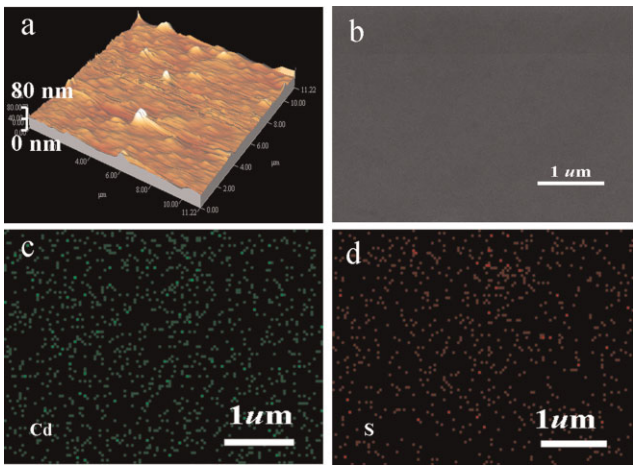

Figure 5 (online colour at: www.pss-a.com) (a,b) Three-dimensional (3D) AFM and FESEM images of ethanedithiol-treated CdS-QDs/P3HT blend film, (c,d) are, respectively, Cd and S EELS mappings of the same region as SEM.

The latter was induced by random leakage current, possibly coming from serious phase separation and some defects in the photoactive layers.

3.4 Morphology characterization of blend film Figure 5a shows AFM topography for 11 μm × 11 μm scan areas of ethanedithiol-treated blend film, indicating the surface was completely covered by blends. However, the topography of the film was slightly rough, exhibiting rough "island" structures from large aggregates of QDs. The obvious film roughness was said to affect the interface contact between the active layer and the electrodes, which suggested a better film morphology needed for high FF. Figure 5b shows the FESEM image of the ethanedithiol-treated film. The SEM image shows the blend film had a smooth surface free from cracks and no obvious phase separation. Figures 5c and d were, respectively, Cd and S elemental EELS mappings of a typical blend film shown in Fig. 5b. The EELS results showed that Cd and S were homogeneously distributed through the film.

4 Conclusions A hybrid solar cell made of CdS-QDs/P3HT blends was fabricated. The bidentate short-chain ligand ethanedithiol was used to treat and assemble the CdS-QDs/P3HT active layer. Ethanedithiol effectively connected nanoparticles both vertically and horizontally and shortened the interdot spacing and thus improved electron transport between QDs. Under AM1.5G illumination, the hybrid solar cell based on ethanedithiol-passivated monolayer blend film had a more than three times increase of PCE over the untreated system. When we assembled a blend film with ethanedithiol by LBL approach, the assembly with a trilayer blend film gained a further improved device performance. The PCE was six times higher than that of the ethanedithiol-passivated monolayer film device. Our work presents a new method to improve the PCE of QDs/polymer hybrid solar cell, which will be more widely applied in solution-processed photovoltaic devices. We believed that the performance of the device could be further enhanced by improving the morphology of the blend film and optimizing the electrode structure, which are currently underway in our laboratory.

Acknowledgements We thank the financial support from the National High Technology Research and Development Program of China (No. 2007AA03Z301), the National Natural Science Foundations of China (No. 20771032, No. 61076040) and Anhui Province (No. 070414200), and the National Basic Research Program of China (No. 2007CB9-36001).

References

[1] A. C. Mayer, S. R. Scully, B. E. Hardin, M. W. Rowell, and M. D. McGehee, Mater. Today **10**, 28–33 (2007).
[2] G. Dennler and C. J. Brabec, in: Socio-Economic Impact of Low-Cost PV Technologies, Organic Photovoltaics, edited by C. Brabec, V. Dyakonov, and U. Scherf (Wiley-VCH, Weinheim, 2008,).
[3] J. Y. Kim, K. Lee, N. E. Coates, D. Moses, T. Q. Nguyen, M. Dante, and A. J. Heeger, Science **317**, 222–225(2007).
[4] N. C. Greenham, X. Peng, and A. P. Alivisatos, Phys. Rev. B **54**, 17628–17631 (1996).
[5] F. Zutz, I. Lokteva, N. Radychev, J. Kolny-Olesiak, I. Riedel, H. Borchert, and J. Parisi, Phys. Status Solidi A **206**, 2700–2708 (2009).
[6] I. Gur, N. A. Fromer, C. Chen, A. G. Kanaras, and A. P. Alivisatos, Nano Lett. **7**, 409–414 (2007).
[7] P. Wang, A. Abrusci, H. M. P. Wong, M. Svensson, M. Andersson, and N. C. Greenham, Nano Lett. **6**, 1789–1793 (2006).
[8] B. R. Saunders and M. L. Turner, Adv. Colloid Interface Sci. **138**, 1–23 (2008).
[9] W. U. Huynh, J. J. Dittmer, W. C. Libby, G. L. Whiting, and A. P. Alivisatos, Adv. Funct. Mater. **23**, 73–79 (2003).
[10] I. Lokteva, N. Radychev, F. Witt, H. Borchert, J. Parisi, and J. Kolny-Olesiak, J. Phys. Chem. C **114**, 12784–12791 (2010).
[11] D. A. R. Barkhouse, A. G. Pattantyus-Abraham, L. Levina, and E. H. Sargent, ACS Nano **2**, 2356–2362 (2008).
[12] E. J. D. Klem, H. Shukla, S. Hinds, D. D. MacNeil, L. Levina, and E. H. Sargent, Appl. Phys. Lett. **92**, 212105–212107 (2008).
[13] X. M. Liu, Y. Jiang, X. Z. Lan, S. Y. Li, D. Wu, T. T. Han, H. H. Zhong, and Z. P. Zhang, J. Colloid Interface Sci. **354**, 15–22 (2011).
[14] W. W. Yu, L. Qu, W. Z. Guo, and X. G. Peng, Chem. Mater. **15**, 2854–2860 (2003).
[15] Z. Liang, K. L. Dzienis, J. Xu, and Q. Wang, Adv. Funct. Mater. **16**, 542–548 (2006).
[16] X. Zhang and J. C. Shen, Adv. Mater. **11**, 1139 (1999).